Settling of Particles beneath Water Waves

IAN EAMES

University College London, London, United Kingdom

(Manuscript received 7 March 2007, in final form 1 April 2008)

ABSTRACT

Considered here is the motion of small particles beneath irrotational water waves. The added mass and inertial forces are shown to be an important role in the mean transport of particles. To leading order, particles are transported with a mean horizontal Stokes drift velocity and sediment with their terminal fall velocity. The combination of a settling velocity and a mean drift transports particles a finite distance forward from their point of release.

1. Introduction

An important environmental problem is how effective waves are in dispersing pollution such as oil or dredged material in coastal regions. The dispersive process depends critically on the type of flow generated by the waves, their amplitude, and the history of the flow. Linear water waves moving in the absence of wind stresses generate a mean streaming flow that may have an irrotational and viscous contribution (Longuet-Higgins 1953). For larger-amplitude waves, the boundary layer separates from the free surface, generating turbulence that diffuses beneath the waves (Hunt et al. 2001). As the wave amplitude increases further, the waves break, generating a large subsurface vortex that diffuses into the bulk of the fluid. The effect of wind stress is observed to also generate a growing boundary layer flow at the free surface, which ultimately breaks to generate a jetlike flow and a cellular flow pattern aligned with the wind stress (Melville et al. 1998). Other processes, such as Langmuir circulation cells (Leibovich 1983), are also important in redistributing heat and matter throughout the upper layer of the ocean (Thorpe 1984).

Stokes drift—a second-order drift velocity of fluid particles in the direction of wave propagation—is a major component of wave-induced transport. Stokes (1847) originally examined the transport of fluid particles by water waves propagating over an infinitely deep body of fluid, and he demonstrated that they execute circular orbits in addition to being transported by a constant drift velocity u^2/c, where u is the average fluid speed beneath the waves moving with speed c. This second-order drift velocity also appears in many other areas of fluid mechanics, such as multiphase flows, and is intimately connected to Darwin's drift (Eames and McIntyre 1999).

The main aim of this paper is to examine the transport of small particles and bubbles by progressive water waves. The mean transport of rigid particles beneath water waves has been studied by Grinshpun et al. (2000), who considered the action of a linear drag force on small particles close to neutral buoyancy. Dispersed material in the ocean (consisting of organic matter, larvae, bubbles, sediment) has a relative density comparable to or less than water. Typical values for the density of material that may be found in the ocean are 1076–1102 kg m^{-3} for larvae [which have diameters of 126–194 μm, estimated from the fall speed given by Krug and Zimmer (2004)), 873–973 kg m^{-3} for crude oil (depending on whether it originates from Texas or Mexico), $\sim$1500 kg m^{-3} for sediment, and zero for bubbles. The density of seawater is typically taken to be 1025 kg m^{-3}. As such, other contributions to the force that governs particle dynamics, such as the added mass and inertial forces, are expected to be important. For neutrally buoyant particles, these additional contributions exactly cancel the contribution from viscous drag and are advected in the same manner as fluid particles. We develop a detailed analysis of how dense particles move on average and confirm the major aspects of our

Corresponding author address: Ian Eames, University College London, Torrington Place, London WC1E 7JE, United Kingdom.

DOI: 10.1175/2008JPO3793.1

results numerically, before drawing our conclusions in section 5.

2. Mathematical model

We examine the motion of small, rigid, spherical particles of diameter d and density ρ_p, moving with velocity $\mathbf{v}$ in a flow $\mathbf{u}$ generated by waves. The force on particles moving in unsteady, inhomogeneous flows has been reviewed many times (see Hunt et al. 1995). The total force consists of a combination of drag and buoyancy, and because the density ratio $\rho_p/\rho < O(1)$, the additional contributions from added mass and inertial forces are also important (see forces reviewed by Magnaudet and Eames 2000). When the Reynolds number, $\mathrm{Re}_p = |\mathbf{v} - \mathbf{u}|d/\nu$ (where ν is the kinematic viscosity of water), based on the relative slip velocity of the particle to the fluid, is smaller than unity, the drag on the particles is viscously dominated and is proportional to the slip velocity. In combination, the particle dynamics are described, to leading order, by the combination of drag, buoyancy, added mass, and inertial forces, expressed as

$$\frac{\mathrm{d}\mathbf{v}}{\mathrm{d}t} = \frac{1}{t_p}(\mathbf{u} - \mathbf{v} - v_T\hat{\mathbf{y}}) + \frac{(1 + C_m)}{\rho_p/\rho + C_m}\frac{\mathrm{D}\mathbf{u}}{\mathrm{D}t}, \quad \frac{\mathrm{d}\mathbf{x}}{\mathrm{d}t} = \mathbf{v}, \quad (1)$$

where C_m is the added mass coefficient and the value of $C_m = 1/2$ is prescribed for a spherical particle. The unity vector $\hat{\mathbf{y}}$ is directed vertically upward. Here, the particle response time is defined as

$$t_p = \frac{d^2(C_m + \rho_p/\rho)}{18\nu}, \quad (2)$$

to account for particle densities close to the density of water (ρ). The fall speed in a stagnant fluid is

$$v_T = \frac{g(\rho_p/\rho - 1)d^2}{18\nu} = \frac{\rho_p/\rho - 1}{C_m + \rho_p/\rho}t_p g. \quad (3)$$

We define the Stokes number to be $\mathrm{St} = \omega t_p$, based on the characteristic particle response time and the wave angular frequency. We apply a further restriction to the particle equation of motion, namely that the particles respond quickly to the changing flow; that is, the ratio of the particle response time to wave period $T = 2\pi/\omega$ is small, thus $t_p/T \ll 1$ or $\mathrm{St} \ll 2\pi$. This criterion ensures that history forces are negligible.

We consider how particles are transported by monochromatic waves of amplitude a, angular frequency ω, and wavenumber k, moving over an infinitely deep body of water. We restrict our attention to two-dimensional waves of steepness $ak < 0.33$ whose irrotational flow is described by

$$\mathbf{u} = \{f(y)[\cos(kx - \omega t), \sin(kx - \omega t)]\}, \quad (4)$$

where

$$f(y) = ack e^{ky}. \quad (5)$$

The wave height is $\zeta = a\cos(kx - \omega t)$ (see Lighthill 1978, p. 208). The speed of wave propagation is $c = \omega/k$. For wavelengths greater than 2 cm, surface tension is not important and the dispersion relation is $\omega^2 = gk$. The analysis can be extended to include capillary forces by modifying the dispersion relation. The dimensionless ratio $\tilde{v}_T = v_T/c$ can be expressed in terms of St as $\tilde{v}_T = (\rho_p/\rho - 1)\mathrm{St}/(C_m + \rho_p/\rho)$, so that $|\tilde{v}_T| < \mathrm{St}$.

Because we are studying the difference between the mean motion of small rigid particles and the mean motion of infinitesimal fluid particles, it is useful to recap Stokes drift velocity v_f^S (where the suffix f refers to fluid particles). The fluid particle Stokes drift velocity is

$$v_f^s = \lim_{t\to\infty}\frac{1}{ct}\int_0^t u^2 \mathrm{d}t \approx (ak)^2 c e^{2ky}. \quad (6)$$

The Stokes drift velocity can be calculated by following fluid particles (in the steady frame moving in the wave frame) using the method of Eames et al. (1994) or Longuet-Higgins (1986), but this requires Eulerian information about the periodic domain of the flow.

The particle response time increases with particle diameter. For the constraint $\mathrm{St} < 2\pi$ to apply, the particle diameter must be smaller than d_m (i.e., $d < d_m$), where the critical diameter is

$$d_m = \left(\frac{18\nu}{C_m + \rho_p/\rho}\right)^{(1/2)}\left(\frac{2\pi\lambda}{g}\right)^{(1/4)}. \quad (7)$$

Figure 1a shows the critical diameter plotted for wavelengths less than 1 m and for density contrasts of $\rho_p/\rho = 0$, 1.5, and 2. For particles sedimenting beneath waves, the slip velocity is largely determined by the particle terminal velocity, and the particle Reynolds number is

$$\mathrm{Re}_p \approx \frac{d|v_T|}{v} = |\rho_p - \rho|\frac{d^3 g}{18\nu}. \quad (8)$$

Figure 1b shows a contour plot of Re_p for varying particle diameter and densities, with the limit $\mathrm{Re}_p = 1$ indicated. Also indicated in Fig. 1b are the approximate regions corresponding to crude oil, sediment, and larvae.

To study how particles move in an oscillatory flow field, we average the particle velocity over a wave period and define $\bar{\mathbf{v}}$ and $\bar{\mathbf{X}}$ as

$$\bar{\mathbf{v}}(t) = \frac{1}{T}\int_{t-T}^{t}\mathbf{v}\mathrm{d}t, \quad \bar{\mathbf{X}}(t) = \frac{1}{T}\int_{t-T}^{t}\mathbf{X}\mathrm{d}t, \quad (9)$$

where $\mathbf{v} = (v_x, v_y)$ and $\mathbf{X} = (X, Y)$. The aim of the following calculations is to distinguish between the

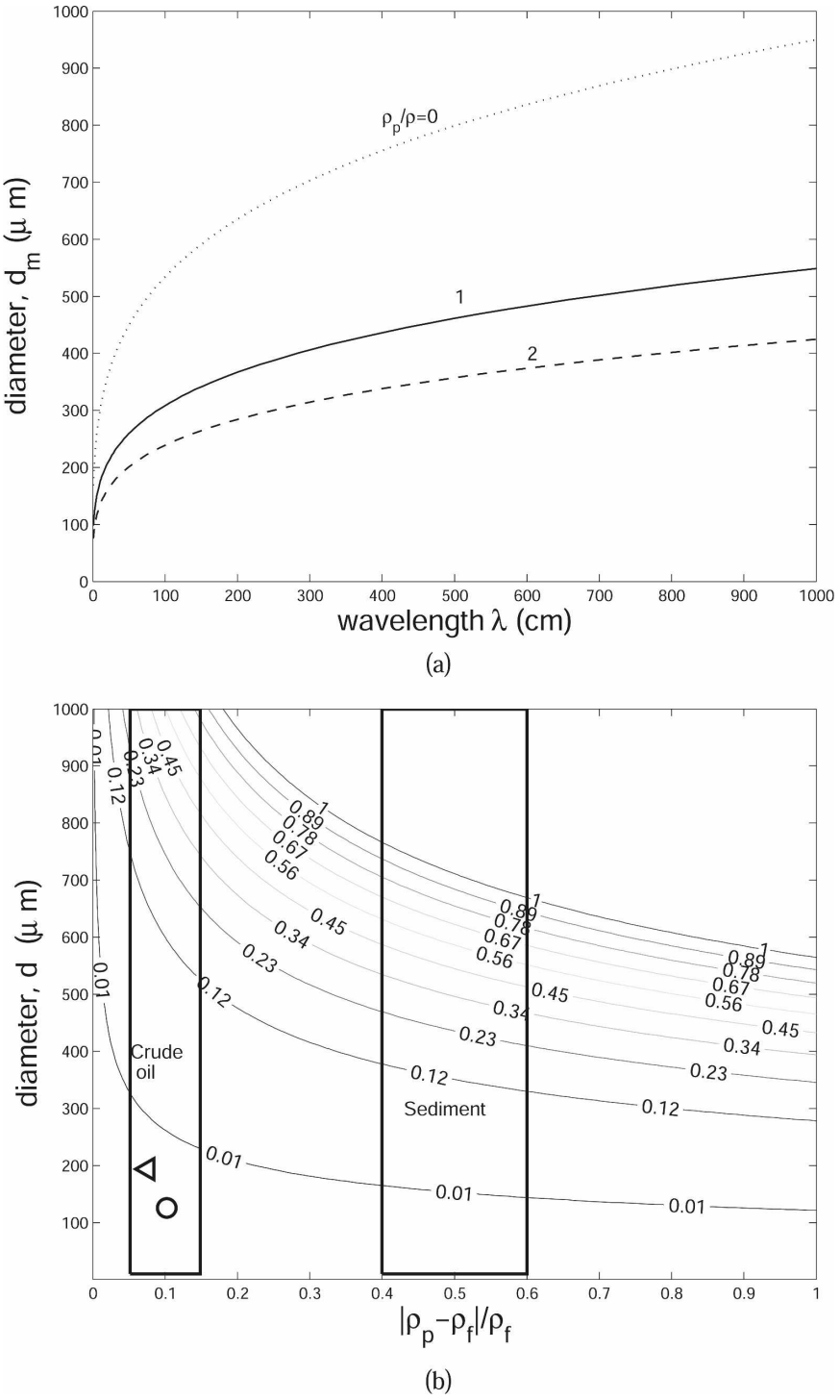

FIG. 1. (a) The region below the full curve shows the parameter regime defined in terms of the maximum particle diameter (d_m) and wavelength (λ) when the particle response time is smaller than the wave period, St = $t_p\omega < 2\pi$. (b) The corresponding criterion requiring the Reynolds number based on the particle terminal fall/rise speed Re_p to be less than unity is plotted. Indicated on the figure are the typical ranges for crude oil, sediment, and the two points corresponding to larvae (from Krug and Zimmer 2004).

mean and oscillatory contributions to the mean particle motion.

3. Analytical calculation of particle dynamics

We employ a weakly inertial approximation $\mathrm{St} \ll 1$ to calculate how particles, released near the free surface, move on average. The weakly inertial approximation essentially converts Lagrangian information about $\mathbf{v}(t)$ into a field variable $\mathbf{v}(\mathbf{x}, t)$ and provides a clear illustration of the differences between the particle and local fluid velocity. We have also explored an alternative approach using complex variables, and this yielded substantially the same results as the weakly inertial approximation.

a. Average particle velocity

For weakly inertial particles $\mathrm{St} \ll 1$ (e.g., Maxey 1987), the particle velocity can be calculated by a series expansion of (1). The particles' sediment relative to the local fluid flow with an inertial correction, given by

$$\mathbf{v} \approx \mathbf{u} - v_T\tilde{\mathbf{y}} + \tau_p\left(-\frac{\mathrm{d}\mathbf{u}}{\mathrm{d}t}\bigg|_{\mathbf{x}_p} + \frac{1 + C_m}{\rho_p/\rho + C_m}\frac{\mathrm{D}\mathbf{u}}{\mathrm{D}t}\right). \quad (10)$$

The acceleration of the fluid following the particles is

$$\frac{\mathrm{d}\mathbf{u}}{\mathrm{d}t}\bigg|_{\mathbf{x}_p} \approx \frac{\mathrm{D}\mathbf{u}}{\mathrm{D}t} - v_T\frac{\partial\mathbf{u}}{\partial y}. \quad (11)$$

Combining (10) and (11), we have

$$\mathbf{v} = \mathbf{u} - v_T\hat{\mathbf{y}} + t_p\left(\frac{1 - \rho_p/\rho}{\rho_p/\rho + C_m}\frac{\mathrm{D}\mathbf{u}}{\mathrm{D}t} + v_T\frac{\partial\mathbf{u}}{\partial y}\right). \quad (12)$$

The divergence of the particle velocity field is

$$\boldsymbol{\nabla}\cdot\mathbf{v} = t_p\boldsymbol{\nabla}\cdot\boldsymbol{\nabla}\left(\frac{1}{2}u^2\right) = \frac{16\pi^2\mathrm{St}\omega(ak)^2(1 - \rho_p/\rho)}{\rho_p/\rho + C_m}e^{2ky}. \quad (13)$$

The divergence of the particle velocity field can be used as a diagnostic to determine whether inertial particle collisions are likely to occur (in the absence of Brownian motion) and has been used in the context of particles sedimenting in turbulence (Reeks 2005) and even in the production of warm rain in the atmosphere (Ghosh et al. 2005). From (13), the particle velocity field has a negative divergence for dense particles, indicating that the wave flow reduces the chance of inertial particle collision occurring for dense particles, but it increases the chance of collision for light particles.

From (12), weakly inertial neutrally buoyant particles (where $\rho_p/\rho = 1$ and $v_T = 0$) move with the same velocity as fluid particles,

$$\mathbf{v} = \mathbf{u}. \quad (14)$$

In contrast, the neglect of added mass and inertial forces by Grinshpun et al. (2000) leads to

$$\mathbf{v} = \mathbf{u} - t_p\frac{\mathrm{D}\mathbf{u}}{\mathrm{D}t}. \quad (15)$$

Equation (15) is an incorrect result because it shows that neutrally buoyant particles are driven away from the free surface.

Substituting the flow field (4) into (12) gives the particle velocity

$$\mathbf{v} = Ace^{kY}[\cos(kX - \omega t + \alpha), \quad \sin(kX - \omega t + \alpha)] + [-(ak)^2v_Te^{2kY} - v_T]\hat{\mathbf{y}}, \quad (16)$$

where

$$A = ak[(1 + \mathrm{St}\tilde{v}_T)^2 + \tilde{v}_T^2]^{1/2}, \quad (17)$$

and the phase difference between the particle and fluid velocity is

$$\alpha = -\tan^{-1}\tilde{v}_T/(1 + \mathrm{St}\tilde{v}_T). \quad (18)$$

For $\mathrm{St} \ll 1$, dense particles move with a slightly faster orbital velocity than fluid particles moving at the same mean depth ($\mathcal{A}/ak > 1$), while light particles move slower than fluid particles (because $\mathcal{A}/ak < 1$). This is because dense particles tend to execute a slightly larger circular trajectory than fluid particles (with the same mean depth), covering a farther distance in one wave period. On first inspection, we see that the pressure variation in the bulk of the fluid ($\boldsymbol{\nabla}p = -\rho\mathrm{D}\mathbf{u}/\mathrm{D}t$) is on average directed away from the free surface, which effectively increases the local buoyancy force on the dense particles increasing their fall speed. For small-amplitude waves, the vertical acceleration of the fluid is small, but near the crests of large-amplitude Stokes waves, it can be significantly larger than g (Longuet-Higgins 1986). The mean particle drift is calculated (to second order) using the first-order correction of the particle displacement to the particle velocity field. To first order, the particle position near the fixed point $(X, Y) = (x_0, y_0)$ is

$$\mathbf{X_1} = \frac{A}{k}e^{ky_0}[-\sin(kx_0 - \omega t + \alpha), \quad \cos(kx_0 - \omega t + \alpha)] + [-(ak)^2v_Te^{2ky_0} - v_T]t\tilde{\mathbf{y}}. \quad (19)$$

To determine how the particles move on average, the particle velocity field is expanded about (x_0, y_0) to give

$$\mathbf{v} \approx \mathbf{v}(\mathbf{x}_0, t) + \mathbf{X}_1\cdot\boldsymbol{\nabla}\mathbf{v}|_{\mathbf{x}_0,t} \quad (20)$$

(Batchelor 1967, p. 361) or

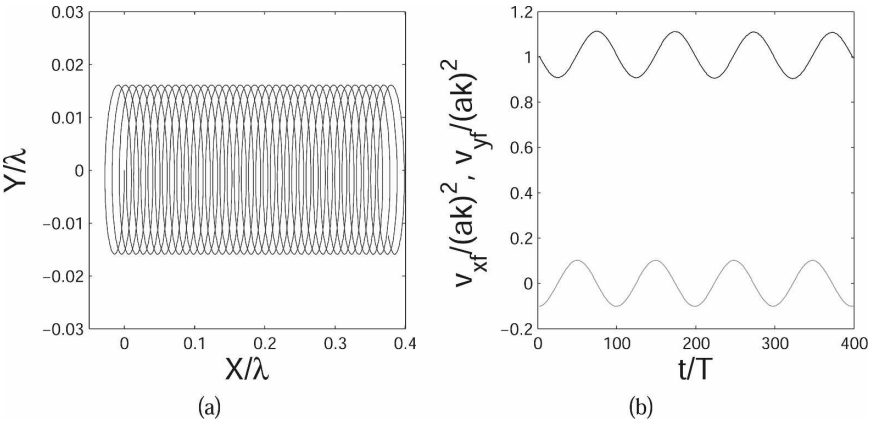

FIG. 2. (a) Trajectory of a fluid particle whose average depth is $y = 0$ and (b) the corresponding average horizontal and vertical velocity at $t = nT$ [defined by (31)].

$$\frac{dX}{dt} = Ace\mathbf{e}^{ky_0}\cos(kx_0 - \omega t + \alpha) + A^2ce\mathbf{e}^{2ky_0} - Ae\mathbf{e}^{ky_0}kv_T t/c\cos(kx_0 - \omega t + \alpha), \quad (21)$$

$$\frac{dY}{dt} = Ae\mathbf{e}^{ky_0}\sin(kx_0 - \omega t + \alpha) - v_T - Ae\mathbf{e}^{ky_0}kv_T t/c\sin(kx_0 - \omega t + \alpha) - (ak)^2 v_T e^{2ky_0}. \quad (22)$$

The particle velocity consists of orbital motion, with a mean horizontal drift velocity

$$v_p^S = \mathrm{A}^2ce^{2ky_0}, \quad (23)$$

sedimentation with the terminal fall velocity, and a contribution due to the correlation between the sedimentation velocity and the orbital fluid flow. The mean horizontal drift velocity—which we refer to as the *particle* Stokes drift velocity—according to these estimates is of the same order as the fluid Stokes drift velocity v_f^S because $\mathcal{A} \sim ak$.

On a longer time scale, we relax the constraint that x_0, y_0 are constant and include the horizontal drift and vertical settling (expressed as $x_0 = v_f^S t$, $y_0 = -v_T t$). Averaging (21) and (22), we obtain

$$\bar{v}_x(t) \approx v_p^S - A^3ce^{3ky_0}\cos\left[(kv_p^S - \omega)t + \alpha - \frac{1}{2}Tkv_p^S\right] + Ae^{ky_0}v_T\sin[(kv_p^S - \omega)t - kv_p^S T + \alpha], \quad (24)$$

$$\bar{v}_y(t) \approx -v_T - A^3ce^{3ky_0}\sin\left[(kv_p^S - \omega)t + \alpha - \frac{1}{2}Tkv_p^S\right] - Av_T e^{ky_0}\cos[kv_p^S(t - T) - \omega t + \alpha] - v_T e^{2ky_0}(ak)^2. \quad (25)$$

For neutrally buoyant particles and fluid particles, the average velocity is

$$\bar{v}_x(t) = v_f^S - (ak)^3ce^{3ky_0}\cos[(kv_f^S - \omega)t + \alpha], \quad (26)$$

$$\bar{v}_y(t) = -(ak)^3ce^{3ky_0}\sin[(kv_f^S - \omega)t + \alpha]. \quad (27)$$

To leading order, neutrally buoyant particles and fluid particles are transported with the Stokes drift velocity [from (26)]. As a consequence of averaging the velocity over a wave period, there is a weak oscillatory component varying on the short time scale T and long time scale T/v_f^S because the particles do not return to their initial position. The long time scale arises from the time it takes for particles to be advected one wavelength. The weak oscillatory component decays much faster with distance y_0 beneath the free surface (as e^{3ky_0}) than v_f^S (which decays as e^{2ky_0}). This is an important result for experimentalists—it means that the horizontal fluid Stokes drift velocity is not equal to the fluid particle velocity averaged over one wave period but rather requires Eulerian information about the wavelength.

For finite-sized particles, the average horizontal velocity is dominated by the particle Stokes drift velocity. The correlation between settling and orbital motion enters as an $O(\mathcal{A}v_T)$ contribution, while the averaging of the Stokes drift velocity introduces an $O(\mathcal{A}^3c)$ contribution, as described above, which dominates over the pressure contribution that scales as $O(\mathcal{A}^2v_T)$. Thus, while the presence of a mean pressure gradient appears to be important in (16), the detailed analysis of the average particle velocity described above shows that it is not.

b. Mean particle transport

From the above analysis, the mean particle velocity is dominated by a horizontal particle Stokes drift velocity

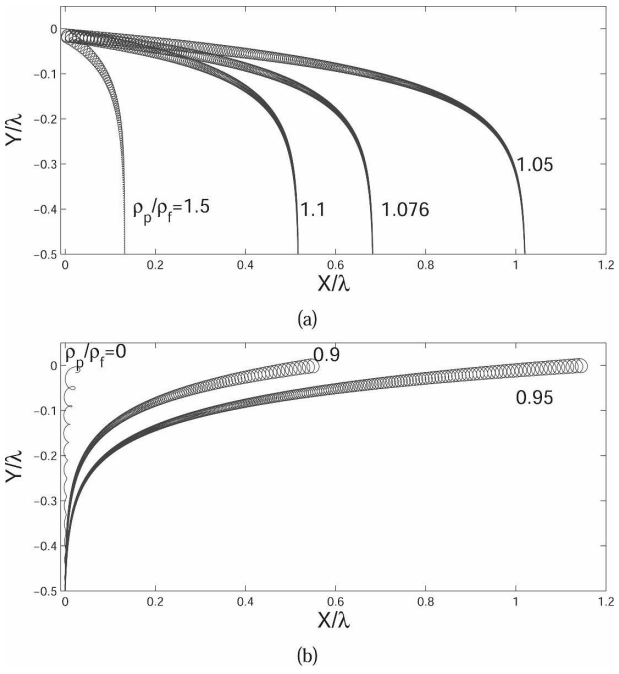

FIG. 3. The trajectories of particles released beneath the wave field are shown in both figures. The Stokes number is fixed at St = 0.02, and wave amplitude $ak = 0.1$. (a) Dense particles are released at the origin; (b) light particles are released at a depth of -0.5λ. The density of the particles is indicated in the figures.

advecting the particle in the direction of the waves and the terminal fall velocity. The average particle position is expressed as

$$\frac{d\overline{\mathbf{X}}}{dt} = v_p^S \hat{\mathbf{x}} - v_T \hat{\mathbf{y}}, \tag{28}$$

where from (23), $v_p^S = v_p^S(0)e^{2k\overline{Y}}$. Integrating (28), a particle released at the origin is transported to

$$\overline{X} = \frac{v_p^S(0)}{2kv_T}(1 - e^{-2kv_T t}), \quad \overline{Y} = -v_T t \tag{29}$$

in time t. From (29), dense particles released at the free surface are permanently displaced a distance

$$X_\infty = \frac{v_p^S(0)}{2k|v_T|} \approx \frac{(ak)^2 g^{1/2}\lambda^{3/2}}{2(2\pi)^{3/2}|v_T|}, \tag{30}$$

forward from their point of release. Light particles released far beneath the free surface are permanently transported a distance X_∞ (given above), before they rise to meet the free surface.

4. Numerical calculations

The equation of motion was integrated, and the positions (X, Y) at $t = nT$, denoted by $X_n = X(nT)$, $Y_n = Y(nT)$, were calculated. The average particle velocity defined by (9) is calculated in terms of its Lagrangian displacements, through

$$\overline{v_x}(nT) = \frac{X_n - X_{n-1}}{T}, \quad \overline{v_x}(nT) = \frac{Y_n - Y_{n-1}}{T}. \tag{31}$$

In the first instance, we consider tracer particles advected by the flow [Eqs. (13), (14)]. Figure 2a shows the trajectories of fluid particles being advected by the wavefield, with the typical looping trajectories beneath the wave ($ak = 0.1$). Figure 2b shows corresponding average velocity based on the fluid particle displacements. The integration was implemented using the Matlab routine ODE113 with an extremely high abso-

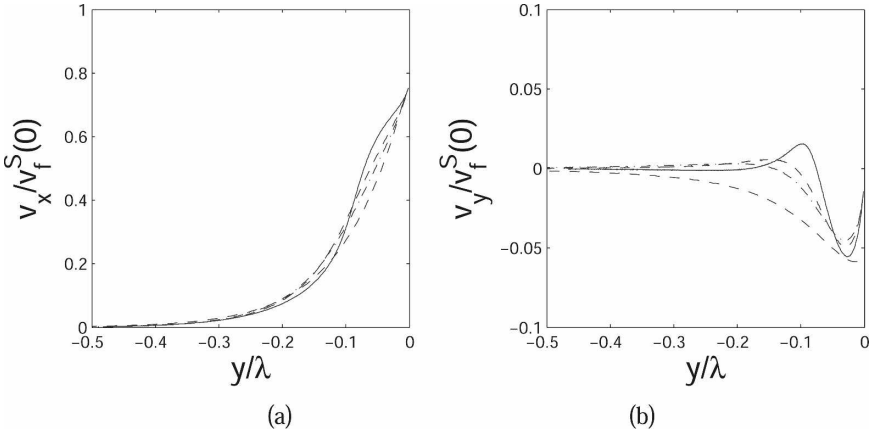

FIG. 4. Numerically calculated (a) average horizontal ($\overline{v}_x$) and (b) vertical particle velocity ($\overline{v}_y + v_T$) of particles corresponding to Fig. 3 are plotted as a function of their vertical position. The full, dashed, dotted–dashed, and dotted curves correspond to $\rho_p/\rho = 1.05$, 1.076, 1.1, and 1.5, respectively.

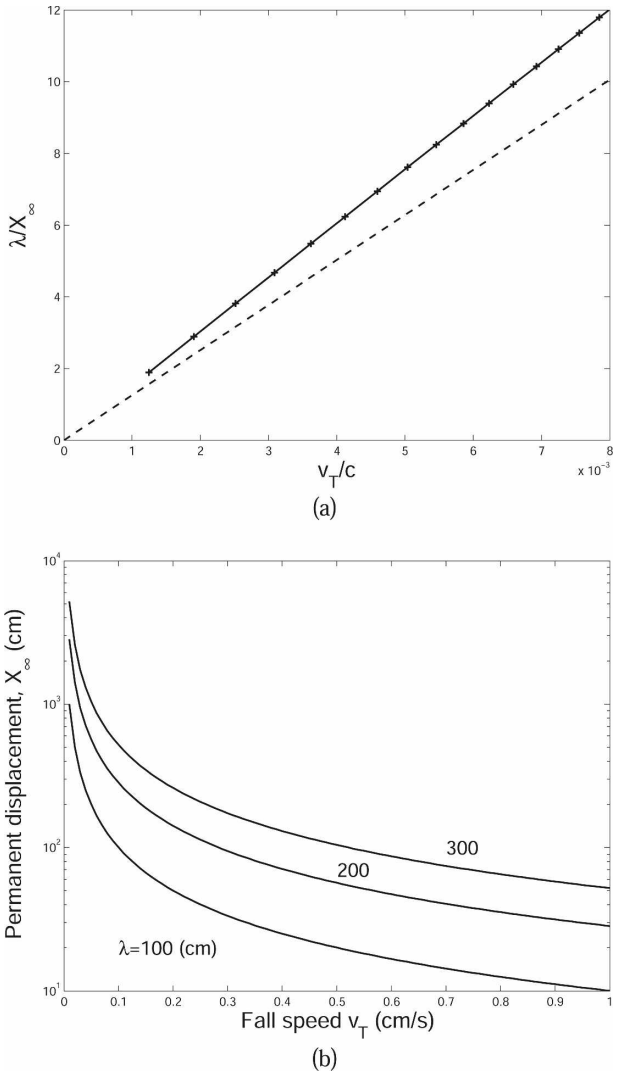

FIG. 5. (a) Comparison between the permanent displacement of dense particles, released at (0, 0), calculated numerically (full line) and (30) (dashed line). The Stokes number is fixed at St = 0.02 and wave steepness at $ak = 0.1$. (b) The permanent forward displacement X_∞ [from (30)] is plotted as a function of fall velocity for wavelengths $\lambda = 100$, 200, and 300 cm and for $ak = 0.1$.

lute tolerance of 10^{-15} to reduce accumulated numerical errors that would otherwise generate a spurious drift velocity. The horizontal and vertical fluid particle velocities were normalized by the fluid Stokes drift velocity at $y = 0$. The average drift velocity calculated from the particle displacement oscillates with a period $T/(ak)^2 \approx 100T$ (for $ak = 0.1$), which corresponds to the time it takes for fluid particles to move one wavelength. This is captured by the analysis in section 3a. In Fig. 2a, the fluid particles are started at $t = T/4$ to ensure that $\overline{Y} = 0$—this is only chosen here to demonstrate that Stokes drift velocity at $y = 0$ is recovered.

Figure 3 shows the trajectories of particles released beneath progressive waves at $t = 0$ for different particle densities (and therefore v_T) for St = 0.02 and $ak = 0.1$ fixed. The orbital motion and settling of the particles are clearly observed, with the particles transported a finite distance forward. In Fig. 3a, dense particles are released at the origin—the densities of $\rho_p/\rho \sim 1.076$ and 1.5 broadly correspond to the release of larvae and sediment. In Fig. 3b, light particles are released far beneath the waves (at a depth of 0.5λ) and correspond to crude oil and bubbles rising for $\rho_p/\rho = 0.95$ and 0, respectively. The numerical calculations were terminated in Fig. 3b when the particles first passed through the free surface. The relationship between particle diameter and wavelength (for a given value of ρ_p/ρ) is $d = \sqrt{18\mathrm{St}\nu/(C_m + \rho_p/\rho)}(\lambda/2\pi g)^{1/2}$. Figure 4a shows the average horizontal particle velocity at $t = nT$, normalized by the fluid Stokes drift velocity at the surface, $[v_f^S(0) = (ak)^2 c]$, and plotted as a function of the particle depth Y_n. The horizontal particle drift velocity decays as the particle sediments, in the same manner as the Stokes drift velocity. The curves in Fig. 4a do not tend to unity (i) because of the presence of the third-order term $O[(ak)^3]$ (evaluated at $t = nT$) in (25) and (ii) because although the particles are released at the origin at $t = 0$, their average position over the first wave period is $y = -\lambda(ak)/4\pi$, sufficiently large so that the Stokes drift velocity is reduced. The difference between the mean vertical particle velocity and the fall velocity $\overline{v_y}(nT) = v_T$ is plotted in Fig. 4b. The mean velocity is dominated by the first three terms in (25), which arise from the averaging of the local flow velocity and the correlation between the fall velocity and the gradients of the fluid velocity. The predictions [Eqs. (24), (25)] quite accurately follow the numerical results of Fig. 4, confirming the detailed analysis.

The permanent-distance dense particles are transported forward from their point of release, are calculated numerically, and are compared to (30) in Fig. 5a. The accuracy of the analytical prediction of permanent-distance particles being transported increases as the sedimentation velocity decreases, as seen by the convergence of the numerical results to the analytical prediction (30), plotted as a dashed line. In Fig. 5b, the predicted permanent displacement (30) is plotted as a function of the particle fall velocity for wavelengths $\lambda =$ 100, 200, and 300 cm and $ak = 0.1$. The permanent displacement increases significantly as the fall velocity decreases and with the square of the wave steepness (ak). Typical values of fall velocity, for larvae, are $v_T =$ 0.1–0.159 cm s^{-1} (Krug and Zimmer (2004)), which indicates that they are permanently transported a dis-

tance 100–600 cm and that this distance increases as the wave steepness increases.

5. Concluding remarks

We have studied analytically and numerically the motion of particles settling beneath progressive irrotational waves. We have shown that added mass and inertial forces must always be included in any description of the particle dynamics because the particle density is typically comparable to (or less than) water—their neglect leads to an analomous vertical drift.

A detailed analysis of the various contributions to the particle velocity averaged over a wave period shows that to leading order, particles are transported with a horizontal particle Stokes drift velocity and sediment with their terminal fall velocity. The particle Stokes drift velocity is slightly smaller than the fluid Stokes drift velocity for dense particles. Weakly inertial, neutrally buoyant particles move the same as fluid particles. Although the oscillatory motion beneath waves generates a near-surface vertical pressure gradient that slightly enhances sedimentation, this is masked (for waves with shallow slopes) by the larger contributions from the correlation between sedimentation and the orbital motion of the fluid and by averaging the orbital motion. Dense particles released near the surface are permanently transported a distance, which scales as $O[(ak)^2 c/k v_T]$.

The analysis presented is built on a simplified description of the force acting on the particles and the flow field. There are instances when additional forces such as a shear-induced lift may be important, for example, within the viscous boundary layers generated at the free surface. For large particles or long fast-moving waves, Re_p and St are no longer small and corrections including a nonlinear drag and history force must be included. When the wave steepness increases, both the Stokes drift velocity and vertical pressure gradient increase significantly (Longuet-Higgins 1986) and are thus likewise expected to increase the mean drift motion of the particles.

Our main conclusion is that to leading order, the average motion of dense particles can be estimated from the particle Stokes drift velocity and their settling velocity, providing a practical method for estimating the influence of waves in transporting particles. Our future research will be to study these processes in the laboratory.

REFERENCES

Batchelor, G., 1967: *An Introduction to Fluid Dynamics.* Cambridge University Press, 635 pp.

Eames, I., S. Belcher, and J. Hunt, 1994: Drift, partial drift, and Darwin's proposition. *J. Fluid Mech.,* **275,** 201–223.

——, and M. McIntyre, 1999: On the connection between Stokes drift and Darwin drift. *Proc. Cambridge Philos. Soc.,* **126,** 171–174.

Ghosh, S., J. Davilla, J. Hunt, A. Srdic, H. Fernando, and P. Jonas, 2005: How turbulence enhances coalescence of settling particles with applications to rain in clouds. *Proc. Roy. Soc. London,* **A461,** 3059–3088.

Grinshpun, S., Y. Redcoborody, S. Kravchuk, V. Zadorozhnii, and V. Zhdanov, 2000: Particle drift in the field of an internal gravity wave. *Int. J. Multiphase Flow,* **26,** 1305–1324.

Hunt, J., R. Perkins, and J. Fung, 1995: Review of the problems of modelling dispersed two-phase flows. *Multiphase Sci. Tech.,* **8,** 595–643.

——, I. Eames, and S. Belcher, 2001: Vorticity dynamics in the water below steep and breaking waves. *Proceedings of Wind over Waves, Mathematics and Its Applications (IMA) Conference,* S. Sajaadi and J. C. R. Hunt, Eds., Ellis Horwood.

Krug, P., and R. Zimmer, 2004: Developmental dimorphism: Consequence for larval behavior and dispersal potential in a marine gastropod. *Biol. Bull.,* **207,** 233–246.

Leibovich, S., 1983: The form and dynamics of Langmuir circulation. *Annu. Rev. Fluid Mech.,* **15,** 391–427.

Lighthill, M. J., 1978: *Waves in Fluids.* Cambridge University Press, 504 pp.

Longuet-Higgins, M., 1953: Mass transport in water waves. *Philos. Trans. Roy. Soc. London,* **245,** 535–581.

——, 1986: Eulerian and Lagrangian aspects of surface waves. *J. Fluid Mech.,* **173,** 683–707.

Magnaudet, J., and I. Eames, 2000: The motion of high-Reynolds-number bubbles in inhomogeneous flows. *Annu. Rev. Fluid Mech.,* **32,** 659–708.

Maxey, M., 1987: The gravitational settling of aerosol particles in homogeneous turbulence and random fields. *J. Fluid Mech.,* **174,** 441–465.

Melville, W., R. Shear, and F. Veron, 1998: Laboratory measurements of the generation and evolution of Langmuir circulations. *J. Fluid Mech.,* **364,** 31–58.

Reeks, M., 2005: On probability density function equations for particle dispersion in a uniform shear flow. *J. Fluid Mech.,* **522,** 263–302.

Stokes, G., 1847: On the theory of oscillating waves. *Trans. Cambridge Philos. Soc.,* **8,** 441–455.

Thorpe, S., 1984: The effect of Langmuir circulation on the distribution of submerged bubbles caused by breaking wind waves. *J. Fluid Mech.,* **142,** 151–169.